

pubs.acs.org/jpr Article

Nanohydrophobic Interaction Chromatography Coupled to Ultraviolet Photodissociation Mass Spectrometry for the Analysis of Intact Proteins in Low Charge States

Molly S. Blevins, Kyle J. Juetten, Virginia K. James, Jamie P. Butalewicz, Edwin E. Escobar, Michael B. Lanzillotti, James D. Sanders, Kyle L. Fort, and Jennifer S. Brodbelt*



Cite This: J. Proteome Res. 2022, 21, 2493-2503



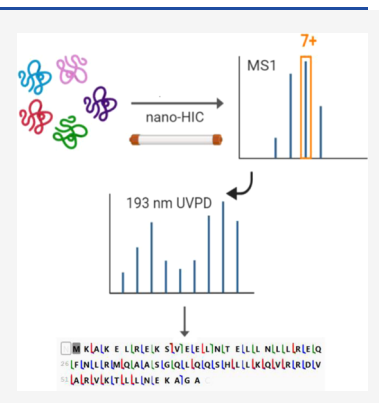
ACCESS I

III Metrics & More

Article Recommendations

s Supporting Information

ABSTRACT: The direct correlation between proteoforms and biological phenotype necessitates the exploration of mass spectrometry (MS)-based methods more suitable for proteoform detection and characterization. Here, we couple nano-hydrophobic interaction chromatography (nano-HIC) to ultraviolet photodissociation MS (UVPD-MS) for separation and characterization of intact proteins and proteoforms. High linearity, sensitivity, and sequence coverage are obtained with this method for a variety of proteins. Investigation of collisional cross sections of intact proteins during nano-HIC indicates semifolded conformations in low charge states, enabling a different dimension of separation in comparison to traditional, fully denaturing reversed-phase separations. This method is demonstrated for a mixture of intact proteins from *Escherichia coli* ribosomes; high sequence coverage is obtained for a variety of modified and unmodified proteoforms.



KEYWORDS: hydrophobic interaction chromatography (HIC), ultraviolet photodissociation (UVPD), mass spectrometry (MS), orbitrap mass spectrometer, protein, proteoform, top-down mass spectrometry (TDMS), native mass spectrometry (nMS), collisional cross section (CCS), liquid chromatography (LC)

INTRODUCTION

The broad field of proteomics has uncovered many insights related to understanding disease pathways and discovery of diagnostic markers. 1-3 Specifically, the characterization of proteoforms—or the sum of protein products that arise from a single gene as a function of alternative splicing, genetic variations, and post-translational modifications (PTM)—is essential for decrypting many biological processes.⁴ The field of mass spectrometry (MS)-based proteomics has emerged as a powerful tool to characterize and differentiate proteoforms, and multiple strategies have been developed to tackle numerous multifaceted problems.5 MS-based proteomic analysis is typically performed via one of three key approaches categorized as bottom-up^{6,7} and middle-down⁸ methods, both of which incorporate proteolysis of proteins prior to analysis, or top-down, 2,4,9,10 which encompasses analysis of intact proteins. All three strategies generally rely on integration of a robust liquid chromatographic separation method (or less commonly, capillary electrophoresis) and tandem mass spectrometry (MS/MS), typically via electrospray ionization (ESI). While proteolysis-based proteomics strategies are capable of detecting protein modifications with high sensitivity, they lack the ability to directly differentiate proteoforms.^{2,4,9,10} Analysis of intact proteins enables separation and direct identification of proteoforms, which are highly relevant to

correlating the biological function of proteins in disease pathways.^{2–4} However, analysis of intact proteins presents new challenges, both in terms of separation and MS/MS characterization, thus motivating the ongoing quest to advance the performance of top-down analysis and options for top-down analysis.

Reversed-phase liquid chromatography (RPLC) is most commonly employed for separation of intact proteins prior to ESI-MS/MS; this mode of chromatography analyzes proteins in their denatured forms with proteins ionized in high charge states. ^{9,11} Several other separation modalities have been explored for analysis of intact proteins by mass spectrometry, ¹² including size-exclusion chromatography (SEC), ^{12–16} ion-exchange chromatography (IEX), ^{17–19} and hydrophobic interaction chromatography (HIC). ^{20–24} Although well-suited for analysis of native proteins using nondenaturing mobile phases, SEC suffers from low-resolution separation and significant sample dilution. ²⁵ IEX typically uses a salt or pH

Received: July 25, 2022 Published: August 31, 2022





gradient, a factor that may alter MS sensitivity throughout the run, but has proven successful for biopharmaceutical applications. 12 HIC has emerged as a promising alternative for analysis of intact proteins in low charge states and has most notably been applied to characterization of intact proteins and monoclonal antibodies at the MS1 level and/or in conjunction with ECD fragmentation. 21,23,24 The exact mechanism of lowcharge-state production via HIC of intact proteins is not fully understood in the context of protein structures, and HIC has not yet been adapted for high-throughput nanoscale separations.^{20–24} One other emerging separation method for intact proteins is capillary electrophoresis, offering high separation efficiency and being well-adapted for native-like proteins owing to the use of a buffered solution for sample migration. ^{26–30} Among these methods, HIC has a number of similarities to conventional reversed-phase methods, using hydrophobic stationary phases and also a salt to mediate interactions between the stationary phases and proteins.

The consideration of the effect of chromatographic separation on protein structures and thus charge state is a critical one in determining the extent of sequence coverage that may be obtained via tandem mass spectrometry. For example, successful characterization of intact proteins via typical dissociation methods like collision-induced dissociation (CID) (including higher-energy collisional dissociation (HCD)) is dependent on high protein charge states due to the reliance of these MS/MS methods on the mobile protons to facilitate production of a broad array of b/y sequence ions. 31-34 In the context of collisional activation of intact proteins, backbone fragmentation may be relatively sparse and often dominant near the terminal ends of proteins, thus resulting in limited sequence coverage that may be suitable for identification of proteins rather than detailed characterization of modified proteoforms. Alternative activation methods, such as electron capture dissociation (ECD), 35-37 electron transfer dissociation (ETD), 37-39 and ultraviolet photodissociation (UVPD), 40,41 or hybrid methods (for example, EThcD, AI-ETD, ET-UVPD, and AI-ECD)⁴²⁻⁴⁶ are promising options for characterization of intact proteins, although most electronbased methods still exhibit a rather notable dependency on charge states. 44,47 UVPD relies on absorption of 193 or 213 nm photons, allowing access to higher-energy fragmentation pathways that result in a combination of a/x-, b/y-, and c/ztype ions that afford broad sequence coverage. 40,48-50 A unique advantage of UVPD for top-down analysis is its lack of charge-state dependence; high sequence coverages of intact proteins have been obtained for folded, native-like proteins in low charge states as well as denatured, highly charged protein ions with UVPD. 51-53 This feature facilitates coupling of UVPD to both denaturing and native separation modes without sacrificing performance. Moreover, the analysis of fragment ions in low charge states from intact proteins offers the added potential benefit of "decongesting" the spectra because fragment ions are produced in lower charge states, spreading them out in the m/z landscape, easing isotope assignments, and facilitating interpretation of spectra.

Here, we have coupled nano-HIC to MS for production of intact proteins in low charge states and characterization of proteins and proteoforms via UVPD. This work investigates the use of alternative nanoscale separation methods to traditional reversed-phase methods for top-down proteomics and to capitalize on the ability of UVPD to characterize protein fragment ions generated in low charge states because of the

solvent composition used for HIC separations. We also investigate the extent to which native protein structures are retained in an attempt to determine the utility of nano-HIC-UVPD in structural biology/native proteomics.

■ EXPERIMENTAL SECTION

Materials

LC-MS grade water, formic acid, acetic acid, and acetonitrile were purchased from Fisher Scientific. Ammonium acetate, magnesium acetate tetrahydrate, lysozyme (chicken egg white), ubiquitin (bovine erythrocytes), ribonuclease A (bovine pancreas), α -lactalbumin (bovine milk), myoglobin (equine skeletal muscle), cytochrome C (equine heart), and superoxide dismutase (bovine erythrocytes) were all purchased from Millipore Sigma. Escherichia coli strain B 70S ribosome was obtained from New England BioLabs (NEB). For LC-MS runs, individual protein samples were diluted into mobile phase starting conditions without prior cleanup. To avoid interference with protein analysis, nucleic acids from the E. coli 70S ribosome sample were precipitated as previously described.⁵⁴ In brief, 1:4 (v/v) of 100 mM magnesium acetate/ribosome and 1:1 (v/v) acetic acid/ribosome were combined. The mixture was incubated for 1 h at 4 °C with subsequent centrifugation at 10 000 rpm for 5 min. The resulting supernatant was removed, and the sample was exchanged into mobile phase starting conditions for LC-MS experiments.

Native Nano-Liquid Chromatography

Nano-HIC experiments were performed on an UltiMate 3000 RSLCnano system (Thermo Fisher Scientific) configured in direct inject mode. Columns were packed in-house with a PolyPENTYL A bulk material (3 μm, 1500 Å, PolyLC) using 75 μ m I.D. capillaries. HIC columns were packed to ~20 cm length. One microliter of the sample was injected onto the house-packed nano-HIC column using a user-defined program (UDP) for autosampler control and sample injection. Mobile phase compositions included 1 M ammonium acetate (MPA) and 20 mM ammonium acetate, 90% ACN (MPB). Both mobile phases additionally contained 0.1% formic acid (FA). The flow rate was held constant at 400 nL/min for the duration of the 78 min method. After an initial 19 min equilibration period at 1% MPB, proteins were eluted by an increase to 99% MPB from 19-49 min. MPB was held at 99% for an additional 10 min (49-59 min) prior to a 19 min reequilibration period (59.001-78 min). For nano-RPLC experiments, a standard trap and elute method was utilized instead of a direct inject method. Trap and analytical nano-RPLC columns were packed to 3.5 and 20 cm length, respectively, with the PLRP-S packing material (5 μ m, 1000 Å, Agilent). The gradient for RPLC comprised of water (MPA) and acetonitrile (MPB), both with 0.1% formic acid. The RPLC gradient started at 2% MPB and increased to 10% MPB over 5 min (0-5 min), then up to 35% MPB (5-25 min), up to 90% MPB (25-35 min), held at 90% MPB (35-40 min), and re-equilibration at 2% MPB (40.001-55 min). The total method runtime was 55 min with a constant flow rate of 300 nL/min. For all experiments, the autosampler was held at 5 °C. The nano-LC columns were at room temperature for all experiments.

Mass Spectrometry

All data were collected using a modified, research-grade Thermo Scientific Q Exactive HF-X Biopharma mass

spectrometer (Bremen, Germany) that was modified by the addition of a 500 Hz, 193 nm coherent ExciStar excimer laser (Santa Cruz, CA) to perform UVPD in the HCD collision cell, as described previously. 55,56 For all direction infusion experiments, an nESI NanoFlex source was utilized. The same source was used for interfacing of a nano-LC column eluent into the mass spectrometer. The source was operated in positive ion mode at 1.2 kV. Tips for nESI were packed in-house using a P-2000 tip puller (Sutter Instruments) and using 1.2 mm OD, 0.69 mm ID borosilicate capillaries. MS1 scan parameters included 2 µscans/scan, 240K resolution, 5e6 AGC target, and 10 ms maximum injection time. MS/MS experiment parameters included 3 µscans/scan, 240K resolution, 1e6 AGC target, 500 ms maximum injection time, n = 5 loop count (i.e., 5 MS/MS scan events per MS1 precursor scan), an isolation window of 1.4 m/z, and an intensity threshold of 8e4. Inclusion lists with precursor m/z values and charge states were utilized for all experiments; precursor ions for inclusion lists were identified via survey MS1 scans. Intact protein mode was utilized for all protein experiments. All UVPD experiments were performed using 3 pulses, 3 mJ per pulse, unless otherwise noted. Collisional cross section (CCS) measurements were carried out using transient decay analysis (TDA) as previously described, in which CCSs were estimated based on ion decay rates in an Orbitrap analyzer, with a pressure calibration based on the 8+ charge state of holo-myoglobin (240K resolution) and with N₂ as the collision gas. HCD experiments were performed using a three-step NCE program (35, 40, and 45 NCE). All MS/MS data for a given precursor ion were averaged over the peak apex using a 50% base-peak cutoff. The resulting total number of scans averaged per precursor varied based on the precursor elution peak width. MS/MS data was deconvoluted with QualBrowser Xtract using the default S/N value of 3. Deconvoluted MS/MS fragments were manually searched against individual protein sequences in ProSight Lite using a 10 ppm mass error tolerance for all assignments. Quantitation of nano-HIC protein peaks for calibration curve generation was created in QualBrowser using automated peak detection with manual integration adjustments as necessary.

■ RESULTS AND DISCUSSION

As HIC typically results in production of proteins in low charge states owing to the nature of the mobile phase, we hypothesized that HIC would integrate well with UVPD-MS owing to the robust performance of UVPD over a range of charge states. Moreover, the orthogonal separation mode compared to conventional reversed-phase methods (more hydrophobic stationary phase, nonpolar/organic mobile phase) offers the prospect of uncovering proteins that might otherwise be obscured. Existing methods for HIC-MS analysis of intact proteins have utilized mobile phases (MPs) containing 1 M ammonium acetate (MPA) and 20 mM ammonium acetate with 50% ACN (MPB). Under the scope of the strategy and facilitate integration with UVPD for high-throughput protein analysis.

After optimization and evaluation of alternative gradients, all subsequent methods used a PolyPENTYL A stationary phase and a flow rate of 400 nL/min (1–99% MPB over 30 min after a 22 min equilibration period). Mobile phases mirrored those used for previously reported HIC-MS applications—MPA: 1 M ammonium acetate and MPB: 20 mM ammonium acetate,

90% ACN. Both mobile phase components additionally contained 0.1% formic acid (FA), as some proteins are not readily detected without this additive, possibly owing to retention on column or ionization suppression. Using these conditions, benchmark protein lysozyme (14.3 kDa) elutes at ~43 min and is readily detected in low charge states (6+ to 8+) (Figure S1). This retention time corresponds to a solution composition consisting of approximately 30% ACN and 670 mM ammonium acetate (34% MPB). Direct infusion of lysozyme in solutions containing 50 mM ammonium acetate indicates that low charge states (primarily 7+ and 8+) are similarly observed regardless of whether the solvent composition is aqueous, aqueous with 0.1% formic acid, 30% ACN, or 30% ACN and 0.1% formic acid (Figure S2a-d). In contrast, lysozyme sprayed from solutions containing 20% ACN or 50% ACN (Figure S2e,f), each with 0.1% formic acid but without 50 mM ammonium acetate (akin to solution compositions prevalent in conventional reversed-phase PLRP-LC used for proteins), show much higher and broader chargestate distributions, with the 9+ charge state most abundant for both solutions and charge distributions ranging from 8+ to 10+ or 7+ to 13+ for the 20 and 50% ACN conditions, respectively. These comparisons suggest that the presence of high salt concentrations (e.g., 50 mM ammonium acetate) results in low charge states even in the presence of an ample supply of protons from formic acid. Based on additional results shown later, there is no compelling evidence that the low charge states are indicative of fully native-like structures, but rather that the low charge states arise from the use of the high salt concentration, which may partially mitigate protein unfolding and/or from the fast kinetics of the interactions between the proteins and the HIC stationary phase, which may be faster than the kinetics of full protein denaturation or shield the proteins from full exposure to the organic solvent.

An equimolar mixture of five proteins, including ubiquitin, lysozyme, ribonuclease A, cytochrome c, and α -lactalbumin, ranging in size from 8.6 to 14.3 kDa (see Table S1), was separated by nano-HIC (400 μ L/min, 1–99% MPB over 30 min). A representative chromatographic trace is shown in Figure 1a, including both the base-peak trace and the extracted ion chromatograms (XICs) for each of the five proteins. The peaks are somewhat broader than the ones observed upon conventional reversed-phase LC (see Figure S3), for example, 2.0 min (RPLC) vs 3.5 min (HIC) peak width for ribonuclease A. This phenomenon is likely a reflection of the heterogeneity of the protein conformations as well as the efficiency of the HIC separation mechanism. Ubiquitin exhibits the poorest chromatographic resolution, which may reflect multiple different conformers and nonuniform interactions with the HIC stationary phase (Figure 1a). 58,59 The dependence of elution in HIC-MS on the hydrophobic accessible surface area (HASA) may be advantageous for the separation of proteins, which are similar in mass, as observed here for lysozyme (14.3 kDa) and α -lactalbumin (14.2 kDa) (Figure 1a). While these proteins differ by only 127 Da in mass (less than 0.9% difference in mass), the difference in HASA is more prominent, as lysozyme has a theoretical HASA of 946 $Å^2$, while α lactalbumin has a larger HASA of 1460 Å², 1.5× greater than that of lysozyme. Theoretical HASA values for all five proteins are shown in Table S2 and correlate directly with the order of elution of these five proteins. The high-resolution separation of proteins of similar masses is challenging with other nano-LC methods such as nano-RPLC, in which denatured proteins of Journal of Proteome Research pubs.acs.org/jpr Article

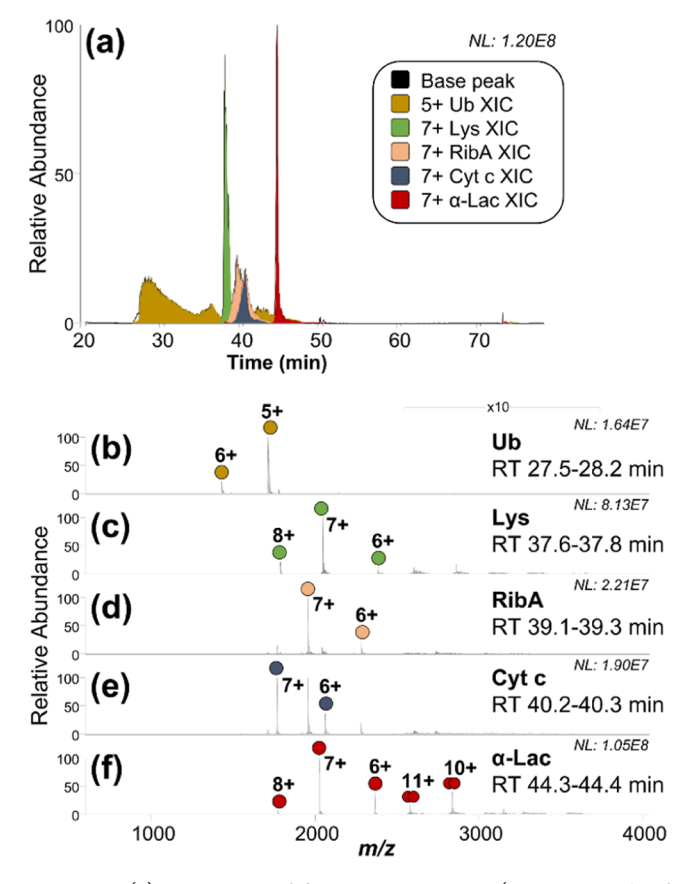


Figure 1. (a) Separation of five protein mixture (12.5 μM each of ubiquitin (Ub), lysozyme (Lys), ribonuclease A (RibA), cytochrome c (Cyt c), and α -lactalbumin (α -Lac)) using nano-HIC/MS with the base-peak chromatogram and extracted ion chromatograms (XICs) of each protein. (b–f) MS1 spectra from the HIC-MS run for each of the five proteins. Nano-HIC separation was performed at a flow rate of 400 nL/min with a 30 min gradient from 1 to 99% MPB.

similar mass often have similar elution times. Development of nanoscale ion-exchange-based chromatographic methods may offer another opportunity for separation of proteins of similar masses and deserve further exploration. 18,19,60–62

Characterization of the five protein mixture was also undertaken using a standard denaturing RPLC approach, for which proteins are generated in higher charge states compared to nano-HIC. The extracted ion chromatograms of the most abundant charge state of each protein is shown in Figure S3a, showing the following order of elution:lysozyme, ribonuclease A, cytochrome c and ubiquitin, and α -lactalbumin. This elution order differs from that observed using nano-HIC (Figure 1a) as the RPLC method separates proteins based on hydrophobicity of denatured proteins, while nano-HIC separates based on the hydrophobic accessible surface area of partially folded proteins. The separation methods are complementary; for example, ubiquitin and cytochrome c, which co-elute by RPLC (Figure S3a), are resolved by HIC (Figure 1a).

As shown in Figure 1b, the MS1 spectra of each of the five proteins obtained from the nano-HIC runs show low charge states for all five proteins. Even the latest eluting protein, α -lactalbumin, which is thus subjected to the most highly organic mobile phase conditions (highest percentage of ACN), displays low charge states. The charge states of α -lactalbumin range from 7+ to 12+ when sprayed from a denaturing solution

(50:50 water/acetonitrile with 0.1% formic acid) without ammonium acetate (Figure S4).

The production of low charge states by HIC has been observed previously in applications using capillary HIC-MS for the analysis of intact proteins and monoclonal antibodies.^{23,2-} In those prior studies, HIC was classified as a quasi nondenaturing mode of chromatography, and the authors concluded that protein elution occurred faster than complete denaturation using certain types of HIC stationary phase materials (such as the one also used in the present work, PolyPENTYL A). Another plausible explanation for the elution of proteins in low charge states is that the high salt concentration maintained during the separation may contribute to protection of the tertiary structure and limit protonation of less accessible basic side chains or ones involved in stabilizing noncovalent interactions such as hydrogen bonds or salt bridges. ^{23,24} The observation of low-protein charge-state distributions does not necessarily equate with native-like, folded structures, for example, low-charge-state distributions can also be achieved by means of proton-transfer reactions (PTRs), conversion of basic lysine side chains to nonbasic carbamylated groups, and the use of basic (high pH) solution conditions.⁵³ However, none of the reagents typically employed for charge reduction of proteins are used in the nano-HIC-MS conditions; thus, the observation of low charge states for proteins analyzed with this method is likely due to the high ionic strength of the high salt mobile phases.

The presence of low-abundance proteoforms exhibiting mass shifts consistent with post-translational modifications was also observed for a few of the proteins. The separation of lowabundance proteoforms of ubiquitin and lysozyme is shown in Figure S5a,b, respectively. For example, an additional proteoform of ubiquitin (m/z 1778, 5+) elutes slightly earlier than the dominant proteoform (Figure S5a). This low-abundance proteoform may correspond to partial ADP ribosylation of the C-terminal glycine residue at position G76, which has been previously reported $(+C_6H_{14}O_{11}P_2, +324.0011 Da)$. Two additional low-abundance proteoforms are observed for lysozyme, with mass shifts corresponding to approximately -14 and +35 Da relative to the primary proteoform (Figure S5b). These findings showcase the ability of nano-HIC-MS to separate low-abundance proteoforms, ones overshadowed using direct infusion methods or denaturing chromatography workflows.

We investigated the quantitative dynamic range of the nano-HIC-MS method by evaluating the extracted ion chromatograms (XICs) generated from successive replicate injections (n = 3) of increasing concentrations of α -lactalbumin (0.5–12.5 μ M), as shown in Figure 2a. Calibration curves were generated for all five proteins; high linearities were obtained ranging from 0.983 to 0.998 (Figure 2b), underscoring the use of nano-HIC-MS for quantitative analysis. Additionally, the different response factors of each protein are evident from the slopes of the calibration curves (Table S3), with ubiquitin showing the highest response factor and cytochrome c showing the lowest response factor. Limit of detection (LOD) and limit of quantitation (LOQ) using nano-HIC-MS were calculated from the calibration curves of each of the proteins, with LOD values ranging from 2.0 to 5.6 pmol (based on the injection amount) and LOQ values ranging from 6.0 to 17.0 pmol (Table S3). These metrics compare favorably to capillary HIC-MS methods, which have shown detection limits in the range of 14.0–58.5 pmol (based on 2 μ L injections of protein (0.1–0.5

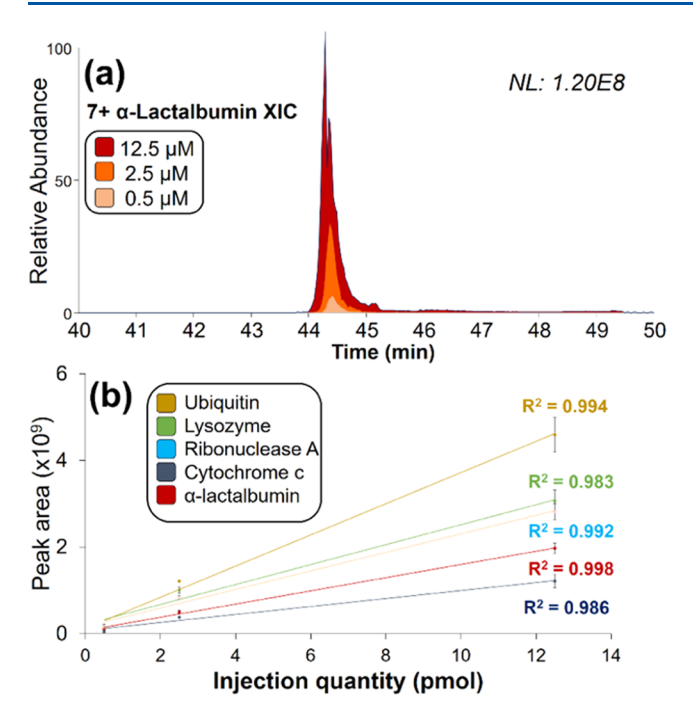


Figure 2. (a) Extracted ion chromatograms of α -lactalbumin (7+) for three 1 μ L injections of 0.5, 2.5, and 12.5 μ M solutions and (b) calibration curves from triplicate injections of 0.5, 2.5, and 12.5 μ M solutions of five proteins with the most abundant charge states used for peak area determination.

mg/mL concentrations, approximately 7-29 µM), oncolumn)²⁴ and benchmark nano-HIC as a sensitive approach. Beyond MS1 detection and quantitation, we evaluated the characterization of the five benchmark proteins via HCD and UVPD. Assessment of HCD and UVPD data via direction infusion resulted in optimal HCD NCE values ranging from 35 to 45 NCE (depending on the protein) and 193 nm UVPD conditions of 3 pulses, 3 mJ per pulse (Figure S6). UVPD conditions which performed best via direct infusion were also shown to perform best using nano-HIC/UVPD-MS (Figure S7). Examples of sequence coverage obtained for the most abundant charge state of lysozyme (7+) are shown in Figure 3a,b, with 40 and 5% sequence coverage using either UVPD or stepped HCD, respectively. Bar graphs of sequence coverage for all five proteins obtained from replicate (n = 3) nano-HIC-MS/MS runs are shown in Figure 3c. Much higher sequence coverage is obtained by 193 nm UVPD compared to HCD. The performance of collisional activation methods like HCD depends greatly on charge states and the presence of mobile protons.³² Collisional activation of proteins in low charge states often results almost exclusively in preferential cleavages (ones adjacent to Pro and/or acidic residues) and thus results in very low sequence coverage.⁶⁵ We have also noted that HCD of proteins in low charge states generated from basic solutions or by carbamylation of lysines results in low sequence coverage.⁵³ Alternative activation methods such as ETD and ECD also perform less proficiently for ions in low charge states because electron activation methods are mediated by the charge density of the targeted ions. 44,66,67 In contrast, 193 nm UVPD generates fragmentation patterns of proteins which are largely charge-independent, thus offering consistently high sequence coverage regardless of charge state. 53,68 UVPD of low-charge-state ions also results in MS/MS spectra in which the fragment ions are more dispersed in the m/z landscape

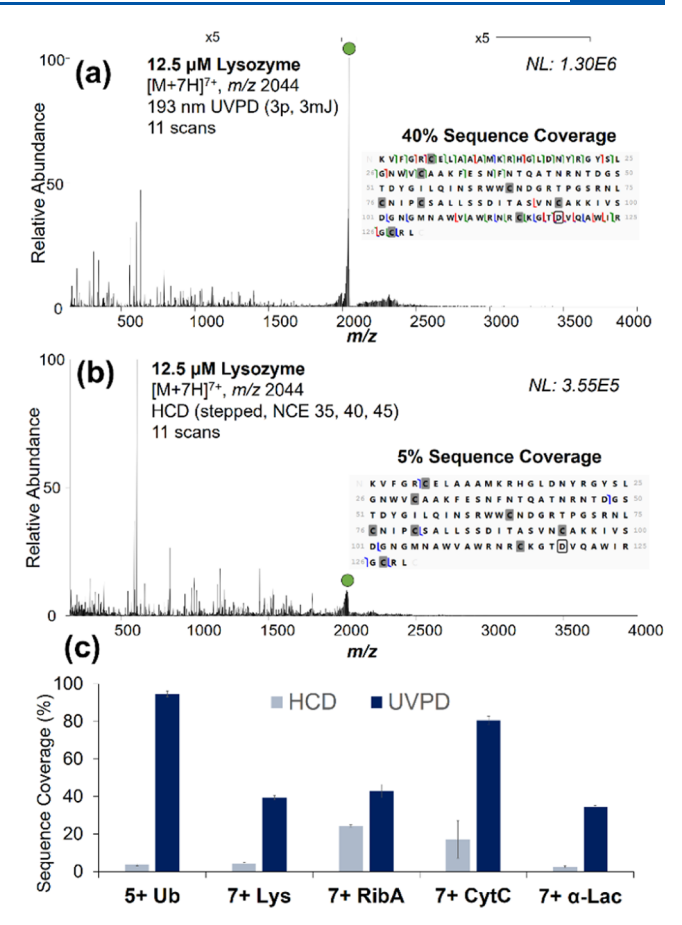


Figure 3. (a) 193 nm UVPD and (b) HCD mass spectra of lysozyme $(7+, m/z \ 2044)$ from representative nano-HIC runs. (c) Comparison of sequence coverage obtained from UVPD and HCD of the most abundant charge states of each of the five proteins via nano-HIC-MS based on the average of replicate experiments (n = 3). The selected precursor is labeled with a green circle. The cysteines involved in disulfide bonds are shaded gray in the sequence maps.

than their respective high-charge-state counterparts, thus often enabling equivalent or even higher sequence coverage and greater levels of characterization. In addition, many of the benchmark proteins included in the present study contain one or more disulfide bonds (Lys: 4, RibA: 4, α -Lac: 4, CytC: 1, Ub: 0). Disulfide-containing proteins are traditionally difficult to characterize via standard MS/MS methods; in contrast, UVPD has been shown to generate high sequence coverage of disulfide-containing proteins owing to the ability of UVPD to cleave disulfide bonds. 69

For the proteins separated by RPLC-MS, sequence coverage obtained by HCD was still somewhat lower than that obtained by UVPD (Figure S3b), but the performance of HCD was significantly better for the same proteins separated by RPLC compared to HIC (Figure 3c) due to the analysis of higher precursor ion charge states. It should also be noted that partial retention of a secondary and/or tertiary structure could affect the sequence coverage results for HCD. This comparison underscores the advantage of UVPD for pairing with HIC separations that are likely to generate low charge states of proteins.

We aimed to further explore whether the conditions used for nano-HIC separation are truly nondenaturing or some intermediate. While low charge states observed for proteins are often indicative of folded, native-like protein structures, they are also characteristic of charge states adopted by proteins in basic solutions and/or may be indicative of collapsed structures. We examined whether noncovalent interactions are maintained by analyzing both myoglobin, which binds its heme ligand via noncovalent interactions, and superoxide dismutase, which exists in a native monomer/dimer equilibrium state. The MS1 spectra obtained from nano-HIC-MS of myoglobin and SOD are displayed in Figure 4a,b, and the

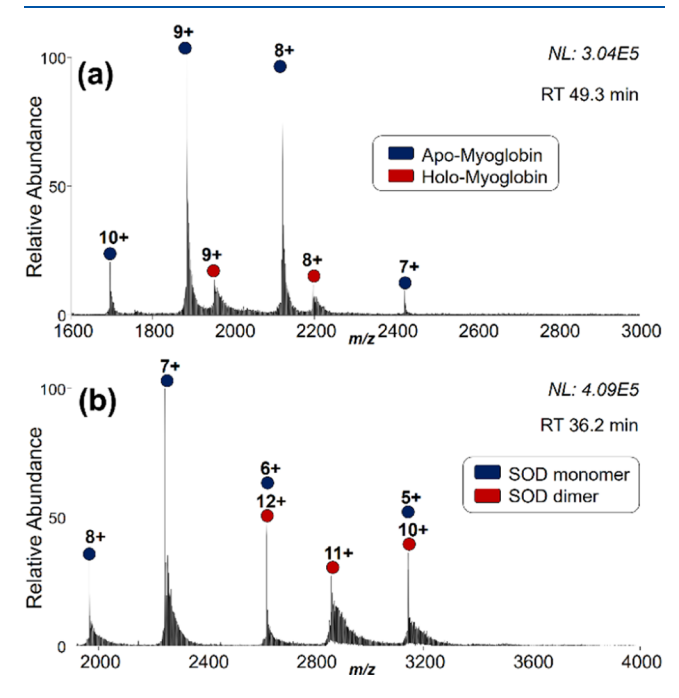


Figure 4. Nano-HIC-LC MS1 spectra obtained for separate 1 μ L injections of 10 μ M solutions containing (a) myoglobin or (b) superoxide dismutase (SOD). The corresponding HIC-LC traces are shown in Figure S8.

companion nano-HIC extracted ion chromatograms of both the monomeric and complexed forms of each protein are displayed in Figure S8. As seen in Figure 4a, the charge-state distribution of myoglobin is low, ranging from 7+ to 10+; however, only a small percentage of the protein retains heme (<10%). SOD displays a majority of monomers (~80% monomers) in the MS1 spectrum, indicating relatively low survival of dimers (20%) (Figure 4b).

The corresponding mass spectra obtained via direct infusion of myoglobin and SOD under native-like solution conditions (high salt concentration, no acid, no organic solvent) are shown in Figure S9. Here, myoglobin is observed solely in its holo heme-bound form, and the distribution of monomeric and dimeric forms of SOD is approximately 58% monomers and 42% dimers. The nano-HIC-MS data implies relatively low survival of noncovalent interactions and is not consistent with a truly "native-like" MS outcome. However, even though the noncovalent interactions are disrupted during migration through the HIC media, the production of low charge states remains dominant. Thus, the high concentration of salt in the mobile phase may suppress protonation, resulting in low charge states and modulating the integrity of noncovalent interactions, which are sensitive to high salt conditions.

In addition to probing the retention of noncovalent interactions using nano-HIC-MS, we also aimed to determine the collisional cross sections (CCSs) of the proteins eluting

from the HIC column. We employed a method previously developed in our group based on the rate of transient signal decay of a protein ion in an Orbitrap mass analyzer. ⁵⁷ In essence, the decay rate of coherent ion motion in an Orbitrap analyzer is directly related to the rotationally averaged size/shape of the ions, thus offering a means to translate decay rate into the CCS. ⁵⁷ Using this methodology, we compared CCS values of the proteins directly eluting from nano-HIC-LC to those infused from native-like solutions (50 mM ammonium acetate) as displayed in Figure 5. The CCS values obtained for

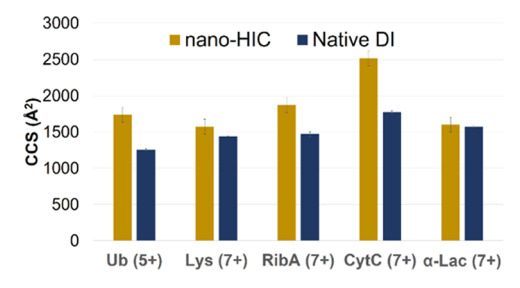


Figure 5. Comparison of collisional cross sections of proteins determined from Orbitrap transient decay measurements from nano-HIC-MS experiments (gold) and direct infusion experiments of individual 12.5 μ M protein solutions containing 50 mM ammonium acetate (navy) (n=3).

the proteins sprayed from native-like solutions correspond well with previously established values; for example, the average CCS value of 1259 Å² for ubiquitin (5+) aligns well with the reported value of 1239 Å² obtained from ion mobility (1.6% deviation).⁷³ In general, the CCS values obtained for the native-like proteins consistently mirror values reported from ion mobility [cytochrome c (7+) (1776 Å² compared to a reported value of 1785 Å², 0.5% deviation)⁷⁴ and lysozyme (7+) (1440 Å² compared to a reported value of 1364 Å², 5.6% deviation)]. The CCS values obtained for the proteins after elution from nano-HIC are generally higher than those obtained for native-like proteins, diverging significantly for ribonuclease A (nearly 300 Å² increase in CCS for HIC), ubiquitin (nearly 500 Å² increase for HIC) and cytochrome c (over 500 Å² increase for HIC). Ubiquitin and cytochrome c have no disulfide bonds to anchor the protein topology, thus indicating that HIC significantly unfolds or elongates these proteins. For the two proteins, α -lactalbumin and lysozyme, each having four disulfide bonds, the CCS values obtained for the proteins eluting from HIC were similar to those obtained upon direct infusion of native-like solutions (HIC and native CCS values within 9% difference). Interestingly, α -lactalbumin and lysozyme also displayed the sharpest chromatographic peaks among the five proteins included in the benchmark mixture, possibly indicating that fewer conformational states are present for α -lactal burnin and lysozyme than the other proteins. Ribonuclease contains four disulfide bonds, but the longest disulfide bond only spans about half of the protein, and its HIC CCS was 27% greater than the native CCS value. Thus, this correlation between the increased CCS values of several of the proteins after HIC and the number of disulfide bonds is consistent with partial unfolding during the HIC elution process. Proteins that are more highly organized via multiple disulfide bonds (such as lysozyme and α -lactalbumin) more readily retain their compact structures and thus yield low CCS values akin to ones expected for more native-like proteins. 76,77 During exposure to the organic solvent (ACN)

Journal of Proteome Research pubs.acs.org/jpr Article

during elution, the proteins lacking significant disulfide bond motifs may partially unfold and adopt intermediate conformational states.

The nano-HIC/MS method was then applied for analysis of a more complex mixture of E. coli ribosomal proteins, along with a comparison to the analysis by conventional reversedphase PLRP-LC. The base-peak traces based on the HIC and PLRP separations are shown in Figure S10, along with extracted ion chromatograms for a selection of 16 representative proteins. Triplicate base-peak LC-MS traces of HIC and RPLC runs are shown in Figure S11 to indicate runto-run reproducibility. Descriptors of the 16 ribosomal proteins are summarized in Figure S10e. As expected, low charge states are observed for the proteins separated by HIC, while much higher charge states are observed in the RPLC separation, for example, 21+ vs 8+ for L13 (16.0 kDa), 15+ vs 7+ for L25 (10.7 kDa), and 10+ vs 5+ for L32 (6.3 kDa) (RPLC vs HIC, respectively). There are major differences in the elution order of different proteins for HIC versus PLRP owing to the aforementioned differences in the basis of separation of these two methods. In certain cases, the resolution of separation is enhanced in nano-HIC in comparison to nano-RPLC. For example, L30 (m/z 802.34, 8+) and L25 (m/z 713.86, 15+), which are slightly overlapping in the RPLC chromatogram $(RT_{max} 29.3 \text{ and } 29.7 \text{ min, respectively, } \Delta RT = 0.4 \text{ min})$ (Figure S10d), are better resolved in the HIC trace shown in Figure S10c (L30 m/z 1282.94, 5+, L25 m/z 1528.56, 7+), which have RT_{max} values of 40.5 and 42.0, respectively (Δ RT = 1.5 min). The same is true of the two overlapping proteins S16 and L18 (RPLC trace in Figure S10d; $RT_{max}\ 33.2$ and 34.1min, respectively) which are better resolved in the HIC trace in Figure S10c (S16 m/z 1532.68, 6+, RT_{max} 42.5 min; L18 m/z1825.02, 7+, RTmax 44.0 min; Δ RT = 1.5 min). While the aforementioned examples describe pairs of proteins which have superior separation resolution via nano-HIC, the majority of proteins from E. coli ribosomes exhibit superior chromatographic resolution via nano-RPLC (Figures S10d vs S10c). Additionally, the overall elution time range across all proteins is shorter for HIC compared to RPLC, indicating a lower overall selectivity. We conclude that the difference in protein elution times, originating from the basis of the difference in selectivity in HIC compared to RPLC, may, in certain cases, be exploited via HIC if insufficient separation is obtained via RPLC. Thus, HIC is presented as a partially complementary technique to RPLC with overall lower selectivity and resolving power, but in some cases improved selectivity and resolution.

Representative UVPD and HCD data in both HIC and RPLC modes showing the MS1 spectra, MS/MS spectra, deconvoluted UVPD, and HCD spectra, and UVPD and HCD fragment maps are shown in Figures S12-S15 for proteins L32, L33, and L29. Examples of assigned product ions from fragment-rich spectral regions are displayed in Figure S16 for proteins L33 and L29. A complete summary of all 16 identified E. coli ribosomal proteins along with monoisotopic masses, protein identifications, UniProt accession numbers, modifications, retention times (HIC and RPLC), sequence coverage (HIC-UVPD, HIC-HCD, RPLC-UVPD, RPLC-HCD), and protein sequences are shown in Table S4. Sequence coverage of the 16 ribosomal proteins is summarized in Figure 6. HCD generates higher sequence coverage (>80%) for 6 out of the 16 major ribosomal proteins in the HIC mode (L30, L33, L31, and L25) compared to the PLRP mode, and UVPD yields higher sequence coverage for four proteins (L30, L33, L34,

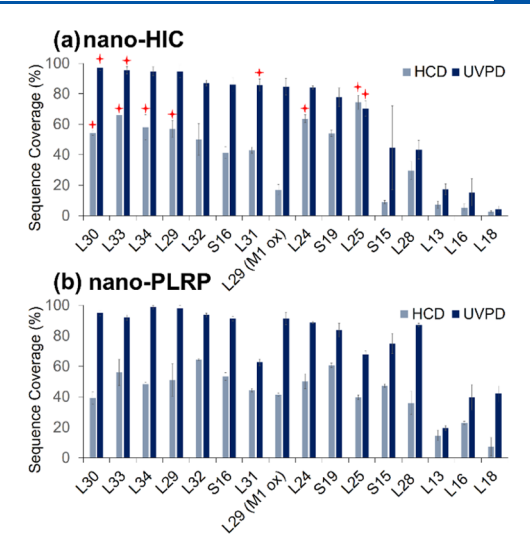


Figure 6. Comparison of sequence coverages obtained by HCD and UVPD for 16 *E. coli* ribosome proteins via (a) nano-HIC and (b) nano-RPLC separation. Stars in panel (a) indicate MS2 conditions for which nano-HIC outperformed nano-RPLC in terms of sequence coverage for UVPD or HCD. Sequence coverages are based on the inclusion of fragment ions from three replicate runs.

L29, L24, and L25) in the HIC mode compared to PLRP-LC. Comparisons of UVPD to HCD indicate that UVPD offers higher sequence coverage for 15 of the 16 proteins in the HIC mode and for all 16 of the proteins in the PLRP mode. However, in most cases, nano-RPLC-UVPD slightly outperforms or is comparable to nano-HIC-UVPD (Figure 6). While, theoretically, HIC-UVPD should outperform RPLC-UVPD due to (1) the independence of UVPD with regard to charge state and (2) the improved spectral decongestion for MS/MS of lower protein ion charge states, the MS/MS data displayed in Figure 6 illustrates that this is not in fact the case. We attribute this discrepancy to the lower initial MS1 signal intensity that is produced using nano-HIC compared to nano-RPLC. Efforts are underway to improve the MS1 signal level of protein ions for nano-HIC-MS via mobile phase modulation. The future aim of obtaining higher MS1 signal levels combined with UVPD will be especially beneficial for HIC separation and analysis of larger proteins, which typically suffer from either low overall sequence coverage (for conventional CID or HCD) or from adequate sequence coverage but spectral congestion (UVPD of high charge states generated by RPLC).

Nano-HIC-UVPD also enables identification of PTMs of some of the ribosomal proteins (Figure S10e). For example, protein L29 was identified both as its Uniprot sequence (m/z 1455.62, 5+) as well as an oxidized form (m/z 1458.82, 5+, Met1 oxidation). This oxidation is localized with confidence given the high sequence coverage of this protein (85% sequence coverage, Figure 6a). The UVPD sequence coverage map for protein L29 with Met1 oxidation is displayed in Figure S17. This PTM identification and localization are also revealed via RPLC/UVPD-MS.

In general, the results demonstrate the high depth of characterization of nano-HIC-UVPD, which is often complementary to nano-RPLC-UVPD, as well as the advantages of an alternative separation modality, which facilitates resolution of certain proteins that may overlap in standard reversed-phase separations. It seems that the retention of partial folding of

proteins during nano-HIC separation enables a different dimension of separation compared to nano-RPLC.

CONCLUSIONS

In this work, we highlight the high sensitivity, linearity, and depth of coverage obtained for separation and characterization of intact proteoforms using nano-HIC/UVPD-MS. UVPD is particularly well suited as an MS/MS method for protein analysis by nano-HIC owing to the low dependence of the performance of UVPD on the ion charge state. Moreover, the low charge states of proteins produced by the HIC solvent composition alleviate some of the spectral congestion often encountered in MS/MS analysis of proteins in high charge states, in which the m/z values of fragment ions are densely spaced. Furthermore, insights are obtained into the nature of the protein structures eluting from HIC, indicating that nano-HIC does not fully preserve native-like conformations but the high salt environment of HIC does mitigate complete denaturation as evidenced by the low charge states and moderately increased collisional cross sections. We view nano-HIC-UVPD-MS as a complementary alternative to more conventional RPLC-based methods, capable of characterizing proteoforms and offering an orthogonal option for expanding protein separation strategies.

ASSOCIATED CONTENT

Supporting Information

The Supporting Information is available free of charge at https://pubs.acs.org/doi/10.1021/acs.jproteome.2c00450.

Nano-HIC-MS base-peak LC-MS trace and MS1 spectrum of lysozyme (Figure S1); direct infusion MS1 spectra of lysozyme using various solvent conditions (Figure S2); nano-RPLC-MS XICs of a standard protein mixture with nano-RPLC-MS and nano-HIC-MS HCD and UVPD protein sequence coverage (Figure S3); native and denaturing α lactalbumin direct infusion MS1 spectra (Figure S4); XICs of ubiquitin and lysozyme low-abundance proteoforms via nano-HIC-MS (Figure S5); sequence coverage plots of ubiquitin and lysozyme via nano-HIC-MS across varying HCD or UVPD conditions (Figure S6); sequence coverage plots for all five standard proteins across varying UVPD conditions (Figure S7); XICs of apo- and holo-myoglobin and monomeric and dimeric SOD via nano-HIC-MS (Figure S8); native direct infusion MS1 spectra of myoglobin and SOD (Figure S9); nano-HIC-MS and nano-RPLC-MS base-peak traces of E. coli ribosome sample with corresponding identified protein XICs and tabulated identification information (Figure S10); base-peak LC-MS traces from nano-HIC and nano-RPLC of the E. coli ribosome sample (Figure S11); example UVPD mass spectra, deconvoluted spectra, and sequence coverage maps of three proteins identified from nano-HIC-UVPD experiments of E. coli ribosome (Figure S12); example HCD mass spectra, deconvoluted spectra, and sequence coverage maps of three proteins identified from nano-HIC-HCD experiments of E. coli ribosome (Figure S13); example UVPD mass spectra, deconvoluted spectra, and sequence coverage maps of three proteins identified from nano-RPLC-UVPD experiments of E. coli ribosome (Figure S14); example HCD mass spectra,

deconvoluted spectra, and sequence coverage maps of three proteins identified from nano-RPLC-HCD experiments of *E. coli* ribosome (Figure S15); example nano-HIC-UVPD spectra of two proteins from *E. coli* ribosome with representative fragment ion assignments (Figure S16); sequence coverage map of *E. coli* ribosomal protein L29, highlighting localization of Met1 oxidation modification (Figure S17); table of the five standard proteins with relevant information (Table S1); table of theoretical hydrophobic accessible surface areas of the five standard proteins (Table S2); table of LOQ and LOD determination from nano-HIC-MS data of standard proteins (Table S3); table of all identified *E. coli* ribosome proteins with comprehensive identification information (Table S4) (PDF)

AUTHOR INFORMATION

Corresponding Author

Jennifer S. Brodbelt — Department of Chemistry, University of Texas at Austin, Austin, Texas 78712, United States;
orcid.org/0000-0003-3207-0217; Email: jbrodbelt@cm.utexas.edu

Authors

Molly S. Blevins — Department of Chemistry, University of Texas at Austin, Austin, Texas 78712, United States

Kyle J. Juetten — Department of Chemistry, University of Texas at Austin, Austin, Texas 78712, United States

Virginia K. James — Department of Chemistry, University of Texas at Austin, Austin, Texas 78712, United States

Jamie P. Butalewicz — Department of Chemistry, University of Texas at Austin, Austin, Texas 78712, United States

Edwin E. Escobar — Department of Chemistry, University of Texas at Austin, Austin, Texas 78712, United States

Michael B. Lanzillotti — Department of Chemistry, University of Texas at Austin, Austin, Texas 78712, United States

James D. Sanders — Department of Chemistry, University of Texas at Austin, Austin, Texas 78712, United States

Kyle L. Fort — Thermo Fisher Scientific, Bremen 28199,

Complete contact information is available at: https://pubs.acs.org/10.1021/acs.jproteome.2c00450

Note:

The authors declare the following competing financial interest(s): The authors declare the following financial interests which may be considered as potential competing interests: one author (Kyle Fort), is an employee of Thermo Fisher Scientific, the developer of the Orbitrap mass spectrometer used for the study.

The authors declare the following financial interests which may be considered as potential competing interests: one author (Kyle Fort) is an employee of Thermo Fisher Scientific Instruments, the developers of the Thermo Scientific Q Exactive HF-X mass spectrometer.

ACKNOWLEDGMENTS

Funding from NSF (CHE-2203602) and the Robert A. Welch Foundation (F-1155) is gratefully acknowledged. Andrew Alpert (PolyLC) is gratefully acknowledged for his chromatography expertise and aid in supplying stationary phase materials. Select graphics were generated with BioRender.com.

REFERENCES

- (1) Angel, T. E.; Aryal, U. K.; Hengel, S. M.; Baker, E. S.; Kelly, R. T.; Robinson, E. W.; Smith, R. D. Mass Spectrometry Based Proteomics: Existing Capabilities and Future Directions. *Chem. Soc. Rev.* 2012, 41, 3912–3928.
- (2) Catherman, A. D.; Skinner, O. S.; Kelleher, N. L. Top Down Proteomics: Facts and Perspectives. *Biochem. Biophys. Res. Commun.* **2014**, *445*, 683–693.
- (3) Gregorich, Z. R.; Ge, Y. Top-down Proteomics in Health and Disease: Challenges and Opportunities. *Proteomics* **2014**, *14*, 1195–1210.
- (4) Melby, J. A.; Roberts, D. S.; Larson, E. J.; Brown, K. A.; Bayne, E. F.; Jin, S.; Ge, Y. Novel Strategies to Address the Challenges in Top-Down Proteomics. J. Am. Soc. Mass Spectrom. 2021, 32, 1278–1294.
- (5) Aebersold, R.; Mann, M. Mass Spectrometry-Based Proteomics. *Nature* **2003**, 422, 198–207.
- (6) Dupree, E. J.; Jayathirtha, M.; Yorkey, H.; Mihasan, M.; Petre, B. A.; Darie, C. C. A Critical Review of Bottom-Up Proteomics: The Good, the Bad, and the Future of This Field. *Proteomes* **2020**, *8*, 14.
- (7) Zhang, Y.; Fonslow, B. R.; Shan, B.; Baek, M.-C.; Yates, J. R. Protein Analysis by Shotgun/Bottom-up Proteomics. *Chem. Rev.* **2013**, *113*, 2343–2394.
- (8) Pandeswari, P. B.; Sabareesh, V. Middle-down Approach: A Choice to Sequence and Characterize Proteins/Proteomes by Mass Spectrometry. *RSC Adv.* **2019**, *9*, 313–344.
- (9) Donnelly, D. P.; Rawlins, C. M.; DeHart, C. J.; Fornelli, L.; Schachner, L. F.; Lin, Z.; Lippens, J. L.; Aluri, K. C.; Sarin, R.; Chen, B.; Lantz, C.; Jung, W.; Johnson, K. R.; Koller, A.; Wolff, J. J.; Campuzano, I. D. G.; Auclair, J. R.; Ivanov, A. R.; Whitelegge, J. P.; Paša-Tolić, L.; Chamot-Rooke, J.; Danis, P. O.; Smith, L. M.; Tsybin, Y. O.; Loo, J. A.; Ge, Y.; Kelleher, N. L.; Agar, J. N. Best Practices and Benchmarks for Intact Protein Analysis for Top-down Mass Spectrometry. *Nat. Methods* **2019**, *16*, 587–594.
- (10) Toby, T. K.; Fornelli, L.; Kelleher, N. L. Progress in Top-Down Proteomics and the Analysis of Proteoforms. *Annu. Rev. Anal. Chem.* **2016**, *9*, 499–519.
- (11) Durbin, K. R.; Tran, J. C.; Zamdborg, L.; Sweet, S. M. M.; Catherman, A. D.; Lee, J. E.; Li, M.; Kellie, J. F.; Kelleher, N. L. Intact Mass Detection, Interpretation, and Visualization to Automate Top-Down Proteomics on a Large Scale. *Proteomics* **2010**, *10*, 3589–3597.
- (12) Füssl, F.; Strasser, L.; Carillo, S.; Bones, J. Native LC-MS for Capturing Quality Attributes of Biopharmaceuticals on the Intact Protein Level. *Curr. Opin. Biotechnol.* **2021**, *71*, 32–40.
- (13) Haberger, M.; Leiss, M.; Heidenreich, A.-K.; Pester, O.; Hafenmair, G.; Hook, M.; Bonnington, L.; Wegele, H.; Haindl, M.; Reusch, D.; Bulau, P. Rapid Characterization of Biotherapeutic Proteins by Size-Exclusion Chromatography Coupled to Native Mass Spectrometry. *MAbs* **2016**, *8*, 331–339.
- (14) Cammarata, M.; Thyer, R.; Lombardo, M.; Anderson, A.; Wright, D.; Ellington, A.; Brodbelt, J. S. Characterization of Trimethoprim Resistant E. Coli Dihydrofolate Reductase Mutants by Mass Spectrometry and Inhibition by Propargyl-Linked Antifolates. *Chem. Sci.* **2017**, *8*, 4062–4072.
- (15) Mehaffey, M. R.; Sanders, J. D.; Holden, D. D.; Nilsson, C. L.; Brodbelt, J. S. Multi-Stage Ultraviolet Photodissociation Mass Spectrometry to Characterize Single Amino Acid Variants of Human Mitochondrial BCAT2. *Anal. Chem.* **2018**, *90*, 9904–9911.
- (16) Shen, X.; Kou, Q.; Guo, R.; Yang, Z.; Chen, D.; Liu, X.; Hong, H.; Sun, L. Native Proteomics in Discovery Mode Using Size-Exclusion Chromatography—Capillary Zone Electrophoresis—Tandem Mass Spectrometry. *Anal. Chem.* **2018**, *90*, 10095—10099.
- (17) Muneeruddin, K.; Nazzaro, M.; Kaltashov, I. A. Characterization of Intact Protein Conjugates and Biopharmaceuticals Using Ion-Exchange Chromatography with Online Detection by Native Electrospray Ionization Mass Spectrometry and Top-down Tandem Mass Spectrometry. *Anal. Chem.* **2015**, *87*, 10138–10145.
- (18) Shi, R. L.; Xiao, G.; Dillon, T. M.; Ricci, M. S.; Bondarenko, P. V. Characterization of Therapeutic Proteins by Cation Exchange

- Chromatography-Mass Spectrometry and Top-down Analysis. MAbs 2020, 12, No. 1739825.
- (19) Murisier, A.; Duivelshof, B. L.; Fekete, S.; Bourquin, J.; Schmudlach, A.; Lauber, M. A.; Nguyen, J. M.; Beck, A.; Guillarme, D.; D'Atri, V. Towards a Simple On-Line Coupling of Ion Exchange Chromatography and Native Mass Spectrometry for the Detailed Characterization of Monoclonal Antibodies. *J. Chromatogr. A* **2021**, *1655*, No. 462499.
- (20) Yan, Y.; Xing, T.; Wang, S.; Li, N. Versatile, Sensitive, and Robust Native LC-MS Platform for Intact Mass Analysis of Protein Drugs. J. Am. Soc. Mass Spectrom. 2020, 31, 2171–2179.
- (21) Wei, B.; Han, G.; Tang, J.; Sandoval, W.; Zhang, Y. T. Native Hydrophobic Interaction Chromatography Hyphenated to Mass Spectrometry for Characterization of Monoclonal Antibody Minor Variants. *Anal. Chem.* **2019**, *91*, 15360–15364.
- (22) Yan, Y.; Xing, T.; Wang, S.; Daly, T. J.; Li, N. Online Coupling of Analytical Hydrophobic Interaction Chromatography with Native Mass Spectrometry for the Characterization of Monoclonal Antibodies and Related Products. *J. Pharm. Biomed. Anal.* **2020**, *186*, No. 113313.
- (23) Chen, B.; Lin, Z.; Alpert, A. J.; Fu, C.; Zhang, Q.; Pritts, W. A.; Ge, Y. Online Hydrophobic Interaction Chromatography—Mass Spectrometry for the Analysis of Intact Monoclonal Antibodies. *Anal. Chem.* **2018**, *90*, 7135–7138.
- (24) Chen, B.; Peng, Y.; Valeja, S. G.; Xiu, L.; Alpert, A. J.; Ge, Y. Online Hydrophobic Interaction Chromatography—Mass Spectrometry for Top-Down Proteomics. *Anal. Chem.* **2016**, *88*, 1885—1891.
- (25) van Schaick, G.; Haselberg, R.; Somsen, G. W.; Wuhrer, M.; Domínguez-Vega, E. Studying Protein Structure and Function by Native Separation–Mass Spectrometry. *Nat. Rev. Chem.* **2022**, *6*, 215–231.
- (26) Belov, A. M.; Zang, L.; Sebastiano, R.; Santos, M. R.; Bush, D. R.; Karger, B. L.; Ivanov, A. R. Complementary Middle-down and Intact Monoclonal Antibody Proteoform Characterization by Capillary Zone Electrophoresis Mass Spectrometry. *Electrophoresis* **2018**, *39*, 2069–2082.
- (27) Bush, D. R.; Zang, L.; Belov, A. M.; Ivanov, A. R.; Karger, B. L. High Resolution CZE-MS Quantitative Characterization of Intact Biopharmaceutical Proteins: Proteoforms of Interferon-B1. *Anal. Chem.* **2016**, *88*, 1138–1146.
- (28) Johnson, K. R.; Greguš, M.; Kostas, J. C.; Ivanov, A. R. Capillary Electrophoresis Coupled to Electrospray Ionization Tandem Mass Spectrometry for Ultra-Sensitive Proteomic Analysis of Limited Samples. *Anal. Chem.* **2022**, *94*, 704–713.
- (29) Shen, X.; Yang, Z.; McCool, E. N.; Lubeckyj, R. A.; Chen, D.; Sun, L. Capillary Zone Electrophoresis-Mass Spectrometry for Topdown Proteomics. *TrAC*, *Trends Anal. Chem.* **2019**, 120, No. 115644.
- (30) Shen, X.; Liang, Z.; Xu, T.; Yang, Z.; Wang, Q.; Chen, D.; Pham, L.; Du, W.; Sun, L. Investigating Native Capillary Zone Electrophoresis-Mass Spectrometry on a High-End Quadrupole-Time-of-Flight Mass Spectrometer for the Characterization of Monoclonal Antibodies. *Int. J. Mass Spectrom.* **2021**, *462*, No. 116541.
- (31) Dongré, A. R.; Jones, J. L.; Somogyi, Á.; Wysocki, V. H. Influence of Peptide Composition, Gas-Phase Basicity, and Chemical Modification on Fragmentation Efficiency: Evidence for the Mobile Proton Model. J. Am. Chem. Soc. 1996, 118, 8365–8374.
- (32) Wysocki, V. H.; Tsaprailis, G.; Smith, L. L.; Breci, L. A. Mobile and Localized Protons: A Framework for Understanding Peptide Dissociation. *J. Mass Spectrom.* **2000**, *35*, 1399–1406.
- (33) Zhang, Z. Prediction of Low-Energy Collision-Induced Dissociation Spectra of Peptides. *Anal. Chem.* **2004**, *76*, 3908–3922. (34) Wells, J. M.; McLuckey, S. A. Collision-Induced Dissociation (CID) of Peptides and Proteins. *Method Enzymol.* **2005**, *402*, 148–185.
- (35) Fort, K. L.; Cramer, C. N.; Voinov, V. G.; Vasil'ev, Y. V.; Lopez, N. I.; Beckman, J. S.; Heck, A. J. R. Exploring ECD on a Benchtop Q Exactive Orbitrap Mass Spectrometer. *J. Proteome Res.* **2018**, *17*, 926–933.

- (36) Greisch, J.-F.; den Boer, M. A.; Lai, S.-H.; Gallagher, K.; Bondt, A.; Commandeur, J.; Heck, A. J. R. Extending Native Top-Down Electron Capture Dissociation to MDa Immunoglobulin Complexes Provides Useful Sequence Tags Covering Their Critical Variable Complementarity-Determining Regions. *Anal. Chem.* **2021**, *93*, 16068–16075.
- (37) Beckman, J. S.; Voinov, V. G.; Hare, M.; Sturgeon, D.; Vasil'ev, Y.; Oppenheimer, D.; Shaw, J. B.; Wu, S.; Glaskin, R.; Klein, C.; Schwarzer, C.; Stafford, G. Improved Protein and PTM Characterization with a Practical Electron-Based Fragmentation on Q-TOF Instruments. J. Am. Soc. Mass Spectrom. 2021, 32, 2081–2091.
- (38) Stoermer, C.; Kaplan, D. A.; Hartmer, R.; Lubeck, M.; Raether, O.; Park, M. A.; Fox, J. Electron Transfer Dissociation on Small Intact Proteins in an Ultra High Resolution Quadrupole Time of Flight Mass Spectrometer. *J. Biomol. Tech.* **2010**, *21*, S38.
- (39) Riley, N. M.; Mullen, C.; Weisbrod, C. R.; Sharma, S.; Senko, M. W.; Zabrouskov, V.; Westphall, M. S.; Syka, J. E.; Coon, J. J. Enhanced Dissociation of Intact Proteins with High Capacity Electron Transfer Dissociation. *J. Am. Soc. Mass Spectrom.* **2016**, 27, 520–531.
- (40) Cleland, T. P.; DeHart, C. J.; Fellers, R. T.; VanNispen, A. J.; Greer, J. B.; LeDuc, R. D.; Parker, W. R.; Thomas, P. M.; Kelleher, N. L.; Brodbelt, J. S. High-Throughput Analysis of Intact Human Proteins Using UVPD and HCD on an Orbitrap Mass Spectrometer. *J. Proteome Res.* **2017**, *16*, 2072–2079.
- (41) Cannon, J. R.; Cammarata, M. B.; Robotham, S. A.; Cotham, V. C.; Shaw, J. B.; Fellers, R. T.; Early, B. P.; Thomas, P. M.; Kelleher, N. L.; Brodbelt, J. S. Ultraviolet Photodissociation for Characterization of Whole Proteins on a Chromatographic Time Scale. *Anal. Chem.* **2014**, *86*, 2185–2192.
- (42) Yu, Q.; Wang, B.; Chen, Z.; Urabe, G.; Glover, M. S.; Shi, X.; Guo, L.-W.; Kent, K. C.; Li, L. Electron-Transfer/Higher-Energy Collision Dissociation (EThcD)-Enabled Intact Glycopeptide/Glycoproteome Characterization. *J. Am. Soc. Mass Spectrom.* **2017**, 28, 1751–1764.
- (43) Cannon, J. R.; Holden, D. D.; Brodbelt, J. S. Hybridizing Ultraviolet Photodissociation with Electron Transfer Dissociation for Intact Protein Characterization. *Anal. Chem.* **2014**, *86*, 10970–10977.
- (44) Riley, N. M.; Westphall, M. S.; Coon, J. J. Activated Ion Electron Transfer Dissociation Enables Comprehensive Top-Down Protein Fragmentation. *J. Proteome Res.* **2017**, *16*, 2653–2659.
- (45) Mikhailov, V. A.; Cooper, H. J. Activated Ion Electron Capture Dissociation (AI ECD) of Proteins: Synchronization of Infrared and Electron Irradiation with Ion Magnetron Motion. *J. Am. Soc. Mass Spectrom.* **2009**, 20, 763–771.
- (46) Rush, M. J. P.; Riley, N. M.; Westphall, M. S.; Coon, J. J. Top-Down Characterization of Proteins with Intact Disulfide Bonds Using Activated-Ion Electron Transfer Dissociation. *Anal. Chem.* **2018**, *90*, 8946–8953.
- (47) Zubarev, R. A. Electron-Capture Dissociation Tandem Mass Spectrometry. *Curr. Opin. Biotechnol.* **2004**, *15*, 12–16.
- (48) Fornelli, L.; Srzentić, K.; Toby, T. K.; Doubleday, P. F.; Huguet, R.; Mullen, C.; Melani, R. D.; dos Santos Seckler, H.; DeHart, C. J.; Weisbrod, C. R.; Durbin, K. R.; Greer, J. B.; Early, B. P.; Fellers, R. T.; Zabrouskov, V.; Thomas, P. M.; Compton, P. D.; Kelleher, N. L. Thorough Performance Evaluation of 213 Nm Ultraviolet Photodissociation for Top-down Proteomics. *Mol. Cell Proteomics* 2020, 19, 405–420.
- (49) R Julian, R. The Mechanism behind Top-Down UVPD Experiments: Making Sense of Apparent Contradictions. *J. Am. Soc. Mass Spectrom.* **2017**, 28, 1823–1826.
- (50) Brodbelt, J. S.; Morrison, L.; Santos, I. Ultraviolet Photodissociation Mass Spectrometry for Analysis of Biological Molecules. *Chem. Rev.* **2020**, *120*, 3328–3380.
- (51) Sipe, S. N.; Brodbelt, J. S. Impact of Charge State on 193 Nm Ultraviolet Photodissociation of Protein Complexes. *Phys. Chem. Chem. Phys.* **2019**, 21, 9265–9276.
- (52) Greer, S. M.; Holden, D. D.; Fellers, R.; Kelleher, N. L.; Brodbelt, J. S. Modulation of protein fragmentation through

- carbamylation of primary amines. J. Am. Soc. Mass Spectrom. 2017, 28, 1587–1599.
- (53) Bashyal, A.; Sanders, J. D.; Holden, D. D.; Brodbelt, J. S. Top-Down Analysis of Proteins in Low Charge States. *J. Am. Soc. Mass Spectrom.* **2019**, *30*, 704–717.
- (54) Hardy, S. J.; Kurland, C. G.; Voynow, P.; Mora, G. Ribosomal Proteins of *Escherichia Coli*. I. Purification of the 30 S Ribosomal Proteins. *Biochemistry* **1969**, *8*, 2897–2905.
- (55) Sanders, J. D.; Shields, S. W.; Escobar, E. E.; Lanzillotti, M. B.; Butalewicz, J. P.; James, V. K.; Blevins, M. S.; Sipe, S. N.; Brodbelt, J. S. Enhanced ion mobility separation and characterization of isomeric glycerophospholipids using absorption mode Fourier transform multiplexing and ultraviolet photodissociation mass spectrometry. *Anal. Chem.* **2022**, *94*, 4252–4259.
- (56) Fort, K. L.; Dyachenko, A.; Potel, C. M.; Corradini, E.; Marino, F.; Barendregt, A.; Makarov, A. A.; Scheltema, R. A.; Heck, A. J. R. Implementation of Ultraviolet Photodissociation on a Benchtop Q Exactive Mass Spectrometer and Its Application to Phosphoproteomics. *Anal. Chem.* **2016**, *88*, 2303–2310.
- (57) Sanders, J. D.; Grinfeld, D.; Aizikov, K.; Makarov, A.; Holden, D. D.; Brodbelt, J. S. Determination of Collision Cross-Sections of Protein Ions in an Orbitrap Mass Analyzer. *Anal. Chem.* **2018**, *90*, 5896–5902.
- (58) Ridgeway, M. E.; Silveira, J. A.; Meier, J. E.; Park, M. A. Microheterogeneity within Conformational States of Ubiquitin Revealed by High Resolution Trapped Ion Mobility Spectrometry. *Analyst* **2015**, *140*, 6964–6972.
- (59) Ujma, J.; Jhingree, J.; Upton, R.; Benoit, F.; Bellina, B.; Barran, P. Protein Unfolding in Freeze Frames: Intermediates of Ubiquitin and Lysozyme Revealed by Variable Temperature Ion Mobility-Mass Spectrometry, Unpublished work.
- (60) Ma, F.; Raoufi, F.; Bailly, M. A.; Fayadat-Dilman, L.; Tomazela, D. Hyphenation of strong cation exchange chromatography to native mass spectrometry for high throughput online characterization of charge heterogeneity of therapeutic monoclonal antibodies. *MAbs* **2020**, *12*, No. 1763762.
- (61) Füssl, F.; Cook, K.; Scheffler, K.; Farrell, A.; Mittermayr, S.; Bones, J. Charge variant analysis of monoclonal antibodies using direct coupled pH gradient cation exchange chromatography to high-resolution native mass spectrometry. *Anal. Chem.* **2018**, *90*, 4669–4676
- (62) Muneeruddin, K.; Bobst, C. E.; Frenkel, R.; Houde, D.; Turyan, I.; Sosic, Z.; Kaltashov, I. A. Characterization of a PEGylated protein therapeutic by ion exchange chromatography with on-line detection by native ESI MS and MS/MS. *Analyst* **2017**, *142*, 336–344.
- (63) Chatrin, C.; Gabrielsen, M.; Buetow, L.; Nakasone, M. A.; Ahmed, S. F.; Sumpton, D.; Sibbet, G. J.; Smith, B. O.; Huang, D. T. Structural Insights into ADP-Ribosylation of Ubiquitin by Deltex Family E3 Ubiquitin Ligases. *Sci. Adv.* **2020**, *6*, No. eabc0418.
- (64) Yan, F.; Huang, C.; Wang, X.; Tan, J.; Cheng, S.; Wan, M.; Wang, Z.; Wang, S.; Luo, S.; Li, A.; Guo, X.; Feng, M.; Liu, X.; Zhu, Y.; Zhou, Y. Threonine ADP-Ribosylation of Ubiquitin by a Bacterial Effector Family Blocks Host Ubiquitination. *Mol. Cell* **2020**, *78*, 641–652
- (65) Stephenson, J. L.; McLuckey, S. A. Simplification of Product Ion Spectra Derived from Multiply Charged Parent Ions via Ion/Ion Chemistry. *Anal. Chem.* **1998**, *70*, 3533–3544.
- (66) Liu, J.; McLuckey, S. A. Electron Transfer Dissociation: Effects of Cation Charge State on Product Partitioning in Ion/Ion Electron Transfer to Multiply Protonated Polypeptides. *Int. J. Mass Spectrom.* **2012**, 330–332, 174–181.
- (67) Good, D. M.; Wirtala, M.; McAlister, G. C.; Coon, J. J. Performance Characteristics of Electron Transfer Dissociation Mass Spectrometry. *Mol. Cell. Proteomics* **2007**, *6*, 1942–1951.
- (68) Shaw, J. B.; Li, W.; Holden, D. D.; Zhang, Y.; Griep-Raming, J.; Fellers, R. T.; Early, B. P.; Thomas, P. M.; Kelleher, N. L.; Brodbelt, J. S. Complete Protein Characterization Using Top-Down Mass Spectrometry and Ultraviolet Photodissociation. *J. Am. Chem. Soc.* 2013, 135, 12646–12651.

- (69) Quick, M. M.; Crittenden, C. M.; Rosenberg, J. A.; Brodbelt, J. S. Characterization of Disulfide Linkages in Proteins by 193 Nm Ultraviolet Photodissociation (UVPD) Mass Spectrometry. *Anal. Chem.* **2018**, *90*, 8523–8530.
- (70) Bakhtiari, M.; Konermann, L. Protein Ions Generated by Native Electrospray Ionization: Comparison of Gas Phase, Solution, and Crystal Structures. *J. Phys. Chem. B* **2019**, 123, 1784–1796.
- (71) Konermann, L.; Douglas, D. J. Unfolding of Proteins Monitored by Electrospray Ionization Mass Spectrometry: A Comparison of Positive and Negative Ion Modes. J. Am. Soc. Mass Spectrom. 1998, 9, 1248–1254.
- (72) Hogan, C. J.; Ruotolo, B. T.; Robinson, C. V.; Fernandez de la Mora, J. Tandem Differential Mobility Analysis-Mass Spectrometry Reveals Partial Gas-Phase Collapse of the GroEL Complex. *J. Phys. Chem. B* **2011**, *115*, 3614–3621.
- (73) Valentine, S. J.; Counterman, A. E.; Clemmer, D. E. Conformer-Dependent Proton-Transfer Reactions of Ubiquitin Ions. *J. Am. Soc. Mass Spectrom.* **1997**, *8*, 954–961.
- (74) Shelimov, K. B.; Clemmer, D. E.; Hudgins, R. R.; Jarrold, M. F. Protein Structure in Vacuo: Gas-Phase Conformations of BPTI and Cytochrome c. J. Am. Chem. Soc. 1997, 119, 2240–2248.
- (75) Valentine, S. J.; Anderson, J. G.; Ellington, A. D.; Clemmer, D. E. Disulfide-Intact and -Reduced Lysozyme in the Gas Phase: Conformations and Pathways of Folding and Unfolding. *J. Phys. Chem. B* **1997**, *101*, 3891–3900.
- (76) McCabe, J. W.; Mallis, C. S.; Kocurek, K. I.; Poltash, M. L.; Shirzadeh, M.; Hebert, M. J.; Fan, L.; Walker, T. E.; Zheng, X.; Jiang, T.; Dong, S.; Lin, C.-W.; Laganowsky, A.; Russell, D. H. First-Principles Collision Cross Section Measurements of Large Proteins and Protein Complexes. *Anal. Chem.* **2020**, *92*, 11155–11163.
- (77) Beveridge, R.; Covill, S.; Pacholarz, K. J.; Kalapothakis, J. M. D.; MacPhee, C. E.; Barran, P. E. A Mass-Spectrometry-Based Framework To Define the Extent of Disorder in Proteins. *Anal. Chem.* **2014**, *86*, 10979–10991.

☐ Recommended by ACS

Collision-Induced Unfolding Studies of Proteins and Protein Complexes using Drift Tube Ion Mobility-Mass Spectrometer

Xueyun Zheng, David H. Russell, et al.

APRIL 27, 2020

ANALYTICAL CHEMISTRY

READ 🗹

Individual Ion Mass Spectrometry Enhances the Sensitivity and Sequence Coverage of Top-Down Mass Spectrometry

Jared O. Kafader, Neil L. Kelleher, et al.

FEBRUARY 07, 2020

JOURNAL OF PROTEOME RESEARCH

READ 🗹

Probing Folded Proteins and Intact Protein Complexes by Desorption Electrospray Ionization Mass Spectrometry

Bin Yan and Josephine Bunch

FEBRUARY 19, 2021

JOURNAL OF THE AMERICAN SOCIETY FOR MASS SPECTROMETRY

READ 🗹

The Coupling of Taylor Dispersion Analysis and Mass Spectrometry to Differentiate Protein Conformations

Jie Hong, Wei Xu, et al.

MARCH 18, 2020

ANALYTICAL CHEMISTRY

READ **C**

Get More Suggestions >